Durham University

Durham Research Online

Deposited in DRO:

29 August 2017

Version of attached file:

Accepted Version

Peer-review status of attached file:

Peer-reviewed

Citation for published item:

Zhang, Y. and Wang, S. and Wang, Q. and Huang, S. L. and Zhao, W. (2017) 'Profile imaging of actual defects in steel plate based on electromagnetic ultrasonic SH guided wave scattering.', Insight : non-destructive testing and condition monitoring., 59 (7). pp. 383-388.

Further information on publisher's website:

https://doi.org/10.1784/insi.2017.59.7.383

Publisher's copyright statement:

Additional information:

Use policy

The full-text may be used and/or reproduced, and given to third parties in any format or medium, without prior permission or charge, for personal research or study, educational, or not-for-profit purposes provided that:

- a full bibliographic reference is made to the original source
- a link is made to the metadata record in DRO
- the full-text is not changed in any way

The full-text must not be sold in any format or medium without the formal permission of the copyright holders.

Please consult the full DRO policy for further details.

Durham University Library, Stockton Road, Durham DH1 3LY, United Kingdom
Tel : +44 (0)191 334 3042 | Fax : +44 (0)191 334 2971
https://dro.dur.ac.uk

Profile imaging of actual defect in steel plate based on electromagnetic ultrasonic SH guided wave scattering

Yu Zhang[a], Shen Wang[a], Qing Wang[b], Songling Huang[a,*] and Wei Zhao[a]

[a]*State Key Lab of Power System, Department of Electrical Engineering, Tsinghua University, 100084, Beijing, China*

[b]*School of Engineering and Computing Sciences, Durham University, DH1 3LE, Durham, United Kingdom*

Abstract. Defects occur almost inevitably during service of steel plate structures. Industrial safety requirements for steel plate structures are increasingly stringent and the need for defect imaging is urgent. This work proposes a profile imaging method aimed at actual defects in steel plate based on electromagnetic ultrasonic SH guided wave scattering. Firstly, a scattering model is proposed based on characteristics of wave scattering employing the rectangular coordinate system. Scattering points and scattering edges are defined and calculated after positions of scattering points are proved to be unique on the condition that the transmitting direction is known. Secondly, detailed procedures of the actual defect profile imaging method are provided, exploiting direction-controllable transmitters and omni-

* Corresponding author: Songling Huang, Tel. /Fax: +86 10 62772131, Email: huangsling@tsinghua.edu.cn

Yu Zhang was born in 1990. He received his bachelor degree from North China Electric Power University in 2013. He is currently pursuing a PhD degree at the Department of Electrical Engineering of Tsinghua University and working on electromagnetic ultrasonic guided wave testing.

Shen Wang was born in 1979. He received his PhD degree from Tsinghua University in 2008. He is currently a Research Assistant with the Department of Electrical Engineering, Tsinghua University. His research interests include nondestructive testing and evaluation, and virtual instrumentation.

Qing Wang received her PhD degree in 2001. She is currently a lecturer in the School of Engineering and Computing Sciences of Durham University. Her research interests include guided wave scattering and simulation.

Songling Huang was born in 1970. He received his PhD degree from Tsinghua University in 2001. Currently, he is a Professor in the Department of Electrical Engineering of Tsinghua University and his research interests include electromagnetic detection and non-destructive evaluation.

Wei Zhao was born in 1956. He received his doctoral degree from the Moscow Power Engineering Institute in 1991. Currently, he is a Professor in the Department of Electrical Engineering of Tsinghua University. His present research interests are in electromagnetic measurement.

directional receivers. Thirdly, an experimental platform on a steel plate with an actual defect is setup. Electromagnetic acoustic transducers based on SH guided waves are applied to stimulate and receive SH waves. The proposed profile imaging method and procedures are conducted on the experimental platform and a profile image of the actual defect is obtained. Then the error between calculated profile and actual profile is defined and displayed on the plane of the rectangular coordinate system. Results show that the profile image almost clings to actual profile of the defect and the average profile error is only 4.3%. The proposed guided wave scattering model and profile imaging method are verified to be able to describe the profile of the actual defect with high-precision in steel plate.

Keywords: Defects, Propagation and scattering, Ultrasonics, Electromagnetics

1. Introduction

Steel plates are widely used in industrial applications, such as floors of oil and gas tanks [1-2]. Various kinds of defects occur almost inevitably during the long-term usage of tank floors [3]. It is necessary to implement a timely and effective detection on these defects to avoid potential oil-gas leakages or even explosions [4]. However, some tank floors cannot be directly reached and some bear quite large areas, so traditional point-to-point detection methods proved to be infeasible or ineffective for these situations [5-6]. Electromagnetic ultrasonic guided wave testing (EUGW) owns advantages of long detection distance by single-ended excitation and 100% cross sectional detection [7-10]. Therefore, EUGW testing is fairly suitable for efficiently inspecting large-area and unreachable tank floors.

As industrial safety requirements for steel plate structures are increasingly stringent, detection of defects only for position information is not enough [11-12]. The profile and size of defects need to be further studied [13-14]. In recent years, EUGW imaging technique has been developed to obtain more detailed information about defects [15-16]. Guided wave tomography imaging exploits an array of transducers to transmit and receive a group of guided wave rays and reconstructs the defect image using the projection data [17-19]. When guided wave encounters defects and strong scattering happens, the effect of scattering will dominate and lead to much artifacts on the reconstruction image of defects, which severely degrades the positioning accuracy and image quality of defects obtained by traditional guided wave imaging methods [20]. Therefore, recently, defects detection methods based on guided wave scattering signals are proposed to overcome the above challenges. Levine exploited block-sparse technique to reconstruct positions of defects based on a multidimensional linear scattering model of Lamb waves [21-22]. The minimum variance imaging method was applied in Hall's work to detect and localize a through-hole and two through-thickness notches according to scattering assumptions in an aluminum plate [23]. Besides, the scattering

http://mc.manuscriptcentral.com/insi

mechanism and related theoretical models were studied by simulation computation and experiments [24-27]. However, most research about detection or imaging based on guided wave scattering are focused on artificial defects, such as the hand-cut notch, glued-on steel rods, etc. And only locations of defects can be specified, but neither profiles nor sizes of defects can be clearly imaged by scattering-based methods. Actual defects are born with complex and diverse profiles, sizes and scattering characteristics. Therefore, it is fairly necessary to investigate the scattering model and develop imaging method for actual defects.

Profile and depth are both important characteristics for defects. In some situations, more attention is paid to profile; while in some other situations, more attention may be paid to depth. At any rate, the accurate reconstruction of profile for actual defects is critical for decision-making of steel plate maintenance and lifetime prediction. Besides, only profile is measured and studied in a lot of research because profile can provide more information about defects. In addition, profile is even more concerned especially for some shallow but large-area defects. Based on the above accepted facts, it is fairly significant to reconstruct the profile of actual defects in steel plate. Therefore, instead of depth, this work will focus on the profile reconstruction for actual defects in steel plate by electromagnetic ultrasonic SH waves.

In this work, a scattering model and a profile imaging method for actual defects in steel plate employing electromagnetic ultrasonic SH waves are proposed. The theoretical analysis of the scattering model is performed. And the detailed procedures of the actual defect profile imaging method based on the scattering model are demonstrated. Besides, an experimental platform on a steel plate is setup to verify the feasibility and accuracy of the scattering model and the profile imaging method.

2. Scattering Model for Profile Imaging of Actual Defects

The scattering model to be investigated in this work takes electromagnetic ultrasonic SH guided waves as demonstration, but it is not confined to any particular guided wave mode,

http://mc.manuscriptcentral.com/insi

because different guided wave modes only affect the propagation velocity for the proposed scattering model. Fig. 1 illustrates the simplified geometric model of guided wave scattering, which is based on the rectangular coordinate system. T represents the position of the guided wave transmitter, P represents the position of the scattering point, and R represents the position of the guided wave receiver. So the vector $\overrightarrow{TP}$ stands for the guided wave that is stimulated from position T and propagates to the scattering point P. And the vector $\overrightarrow{PR}$ stands for the reflected guided wave from the scattering point P to the receiver R. The straight-line distance between the transmitter and the receiver is $\left|\overrightarrow{RT}\right|$. The vector $\overrightarrow{PE}$ represents the direction of the assumed scattering edge of the scattering point P.

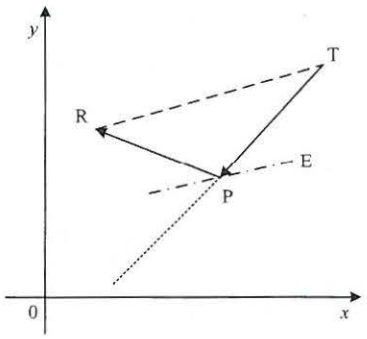

FIG. 1. The simplified geometric model of guided wave scattering on the rectangular coordinate system.

In the simplified geometric model, the positions of the transmitter and the receiver, i.e. T and R, are known quantities. The direction-controllable electromagnetic acoustic transducer (EMAT) is employed as the transmitter in this model, so the direction of the vector $\overrightarrow{TP}$ is also a known quantity, and the angle $\angle$RTP is known. The scattering point P is always on the straight line TP, so as long as the length of the vector $\overrightarrow{TP}$ is determined, the position of the scattering point P will be uniquely determined. Besides, the total propagation time of guided waves from position T, scattered by position P, and finally to position R, can be measured as

http://mc.manuscriptcentral.com/insi

t_r. The propagation velocity of guided waves is v, so the propagation distance can be determined as

$$\left|\overrightarrow{TP}\right| + \left|\overrightarrow{PR}\right| = v * t_r . \tag{1}$$

In the triangle △TPR, according to the law of cosines, the length of the vector $\overrightarrow{PR}$ is calculated as

$$\left|\overrightarrow{PR}\right| = \sqrt{\left|\overrightarrow{TP}\right|^2 + \left|\overrightarrow{RT}\right|^2 - 2 * \left|\overrightarrow{TP}\right| * \left|\overrightarrow{RT}\right| * \cos(\angle RTP)} . \tag{2}$$

So the total propagation distance f, as the function of $\left|\overrightarrow{TP}\right|$, can be expressed as

$$f(\left|\overrightarrow{TP}\right|) = \left|\overrightarrow{TP}\right| + \sqrt{\left|\overrightarrow{TP}\right|^2 + \left|\overrightarrow{RT}\right|^2 - 2 * \left|\overrightarrow{TP}\right| * \left|\overrightarrow{RT}\right| * \cos(\angle RTP)} . \tag{3}$$

In order to prove that one value of f corresponds to only one value of $\left|\overrightarrow{TP}\right|$, the derivative is calculated as

$$\frac{df}{d\left|\overrightarrow{TP}\right|} = 1 + \frac{\left|\overrightarrow{TP}\right| - \left|\overrightarrow{RT}\right| * \cos(\angle RTP)}{\sqrt{\left|\overrightarrow{TP}\right|^2 + \left|\overrightarrow{RT}\right|^2 - 2 * \left|\overrightarrow{TP}\right| * \left|\overrightarrow{RT}\right| * \cos(\angle RTP)}} > 0 . \tag{4}$$

It can be proved that this derivative is always greater than 0, so the propagation distance is a monotonically increasing function of $\left|\overrightarrow{TP}\right|$. And if a certain value of the propagation distance is given, $\left|\overrightarrow{TP}\right|$ can be uniquely determined. And the propagation distance is given by the total propagation time of guided waves. So the formula can be expressed as

$$v * t_r = \left|\overrightarrow{TP}\right| + \sqrt{\left|\overrightarrow{TP}\right|^2 + \left|\overrightarrow{RT}\right|^2 - 2 * \left|\overrightarrow{TP}\right| * \left|\overrightarrow{RT}\right| * \cos(\angle RTP)} . \tag{5}$$

In the formula, only $\left|\overrightarrow{TP}\right|$ is the unknown quantity. By solving the above formula, the position of the scattering point P can be uniquely determined, as well as the propagation and

http://mc.manuscriptcentral.com/insi

scattering paths of guided waves. The direction of the assumed scattering edge $\left.\frac{dy}{dx}\right|_P$ can be calculated as

$$\left.\frac{dy}{dx}\right|_P = \tan\left[\arctan(\left.\frac{dy}{dx}\right|_{\overline{PT}}) - (\frac{\pi}{2} - \frac{1}{2} * \angle TPR)\right]. \quad (6)$$

The calculated scattering point and scattering edge can describe the corresponding local profile of the actual defect. The actual defect profile imaging will be conducted by arranging the EMAT array around the defect. If enough number of scattering points and scattering edges are obtained, the profile image of the defect can be generated.

3. Procedures of Profile Imaging Based on Scattering Model

The EMAT array composed of direction-controllable transmitters and omni-directional receivers will be employed for the profile imaging of the actual defect. The procedures of profile imaging based on scattering model are proposed as the following steps:

1) The direction-controllable transmitters and omni-directional receivers are uniformly mounted around the defect area in a circular shape, and the number of them are respectively N and M. The numbers of omni-directional receivers between any two adjacent transmitters are the same, and the numbers satisfy the relationship M=K*N, where N, M and K are all positive integers. The transmitting angle range of transmitters is θ_1~θ_2, and the angle step is θ_s, so the total number of transmitting angles is $L=(\theta_2-\theta_1)/\theta_s+1$.

2) Select the n^{th} direction-controllable EMAT as the transmitter T_n for this time of detection, where n=1,2,…,N.

3) Select the transmitting angle θ_l of the transmitter in Step 2, and guided waves are stimulated by this transmitter on the selected direction, where l=1,2,…,L.

4) The guided wave detection signals are received by M1 receivers and these receivers are represented as R_{m1}, where $m1$=1,2,…,M1. The time-of-flight t_r that guided waves actually take

http://mc.manuscriptcentral.com/insi

from T_n to R_{ml} is measured by the time-frequency energy density precipitation method [28]. The propagation velocity of guided waves is v. As the geometric model in Fig. 1, the position of the transmitter is T and the position of the receiver is R. The theoretical time-of-flight t_s that guided waves take directly from T to R in the straight line is

$$t_s = \frac{\left|\overrightarrow{TR}\right|}{v}. \tag{7}$$

If $t_r > t_s$, the transmitter T_n and the receiver R_{ml} can form the scattering group (T_n, R_{ml}), and Step 5 is performed; otherwise, if $t_r \leqslant t_s$, the transmitter and the receiver cannot form the scattering group, then Step 7 is performed.

5) For the scattering group (T_n, R_{ml}), Eq. (5) is exploited to calculate the position P of the scattering point.

6) Based on the calculated scattering point position P and the positions of the scattering group (T_n, R_{ml}), Eq. (6) is exploited to calculate the direction of the scattering edge.

7) Judge whether all the transmitting angles have been selected to stimulate guided waves, if they do, Step 8 is performed; if they do not, the transmitting angle θ_{l+1} is taken into consideration and the procedure returns to Step 3.

8) Judge whether all the transmitters have been selected to stimulate guided waves, if they do, Step 9 is performed; if they do not, the transmitter T_{n+1} is taken into consideration and the procedure returns to Step 2.

9) Totally S scattering points are obtained, where S is a positive integer. The position of the i^{th} scattering point is P_i (x_i, y_i), where i=1,2,…,S. All the scattering points are fitted into a curve $D(x)$ based on their own scattering edges

$$D(x) = \arg\left(\min \sum_{i=1}^{S} \left|\varphi(x_i) - y_i\right|^2 \ s.t. \left.\frac{d\varphi}{dx}\right|_{P_i} = \left.\frac{dy}{dx}\right|_{P_i}\right), \tag{8}$$

where $\varphi(x)$ is the fitting function.

http://mc.manuscriptcentral.com/insi

Fig. 2 illustrates the procedures of the profile imaging method of actual defects based on the scattering model.

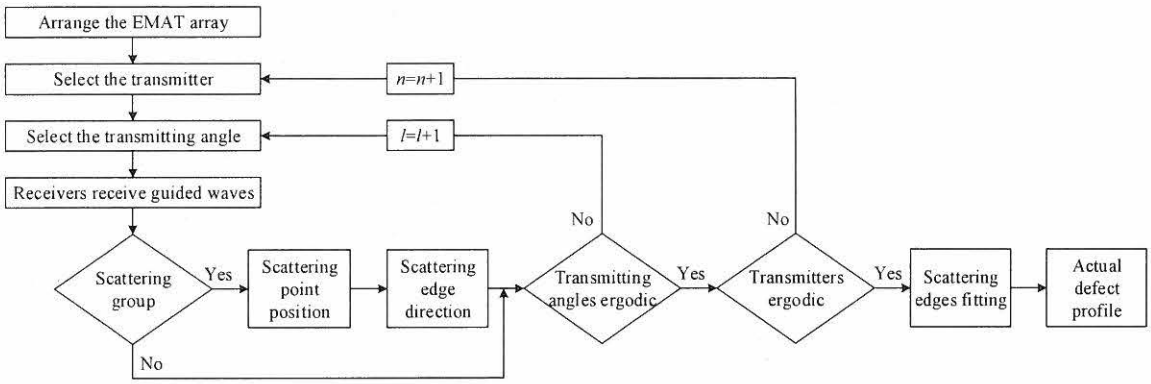

FIG. 2. Theoretical procedures of the actual defect profile imaging method based on the scattering model.

The proposed profile imaging method exploits the scattering characteristic and collects information of the defect boundary, based on the simplified guided wave scattering model. This method is expected to be able to generate high-precision profile images for actual defects.

4. Experiments and Results

The experimental platform on a 4 mm thick steel plate is setup for the actual defect profile imaging. Fig. 3 illustrates the schematic diagram of the experimental platform. Four direction-controllable transmitters [29] and twenty omni-directional receivers are uniformly distributed in a circular shape on the steel plate. And there are five receivers between any two adjacent transmitters. The absolute value of the transmitting angle range is 0° ~80°, and the angle step is 8°, so there are 11 transmitting angles for each transmitter and totally 44 transmitting angles for the experiment. The profile and size of the defect in the steel plate come from an actual corrosion defect in a tank floor plate. The actual profile was measured by a transparent scale paper to obtain its coordinates. And the defect is created with a uniform depth of 1.5

http://mc.manuscriptcentral.com/insi

mm in the test steel plate. This work will only focus on the reconstruction for the profile of the actual defect.

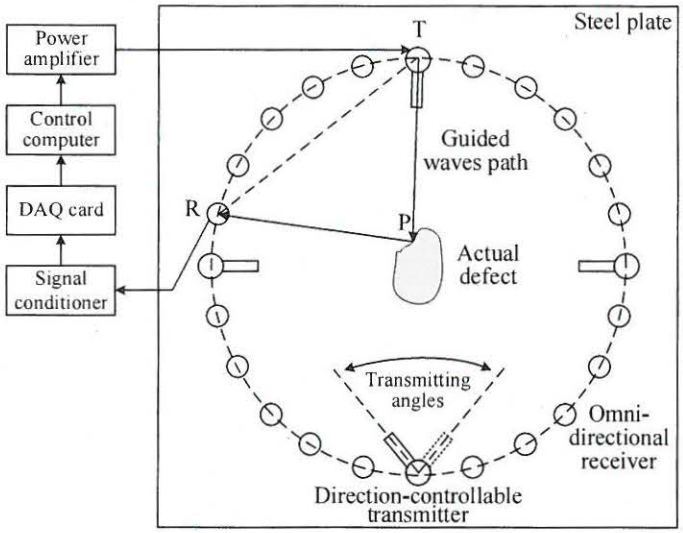

FIG. 3. The schematic diagram of the experimental platform for actual defect profile imaging.

Shear horizontal (SH) guided waves are generated by the transmitter in the steel plate based on magnetostriction. Fig. 4 shows the group velocity dispersion curves of SH waves in a 4 mm thick steel plate. The working frequency is selected as 320 kHz, where only SH0 mode wave exists. SH0 mode wave is free of dispersion and the propagation velocity of SH0 wave in the steel plate is 3200 m/s.

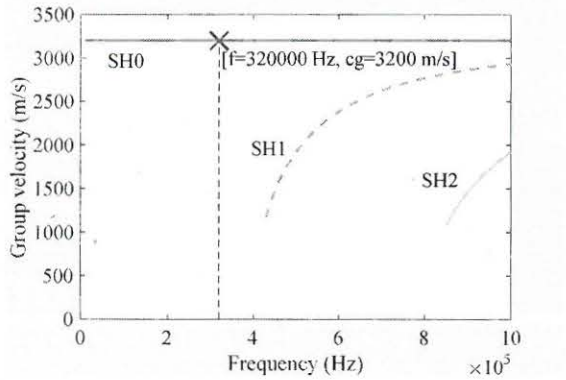

FIG. 4. The group velocity dispersion curves of SH waves in a 4 mm thick steel plate.

http://mc.manuscriptcentral.com/insi

The transmitter is excited by the power amplifier, whose excitation parameters such as the excitation frequency, excitation voltage, the number of excitation cycles are configured by the control computer. SH guided waves are generated in the steel plate and propagate on the preset direction. The receiver receives the guided waves and converts the wave signals into electrical signals. Then the detection signals are sent to the signal conditioner to be filtered and amplified. The processed signals are collected by the data acquisition card to form the detection data. And the detection data is sent to the control computer to be analyzed.

The four transmitters are respectively excited by the power amplifier on preset directions and all the receivers are responsible for receiving guided waves for each time of stimulation, according to the proposed procedures of the profile imaging method. For each time of stimulation, the excitation voltage is 80 V, the excitation frequency is 320 kHz and the number of cycles is 10. The center frequency of the filter in the signal conditioner is also 320 kHz. All the experimental configuration and parameters for each time of detection are the same to avoid the unconformity due to experimental factors.

Based on the procedures of the profile imaging method and the judgement rule for scattering groups, totally 31 scattering points are obtained. The positions of the scattering points and directions of scattering edges are calculated. The scattering points are connected by the fitting curve in the rectangular coordinate system, based on the directions of the scattering edges to form the calculated profile. Fig. 5 illustrates the actual defect profile and the calculated profile in the rectangular coordinate system.

http://mc.manuscriptcentral.com/insi

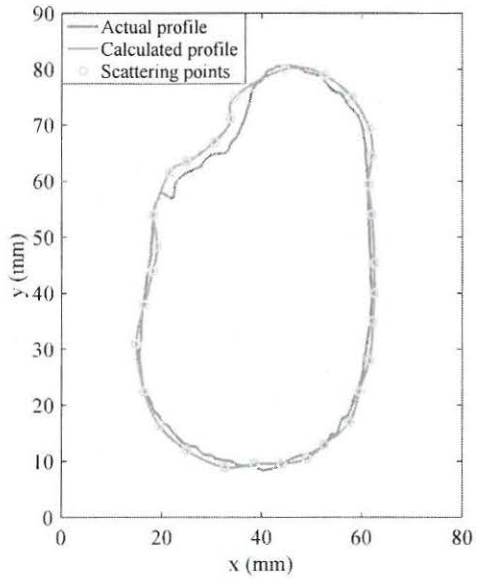

FIG. 5. The profile imaging result of the actual defect.

The calculated profile in Fig. 5 is quite similar with the actual defect profile, and the majority of scattering points are in the near areas of the actual profile. Some scattering points on the top-left of the calculated profile deviate from the actual one for a relatively larger distance.

5. Discussion

In order to evaluate the accuracy of the profile imaging result and analyze the relative influencing factors, the error between the calculated profile and the actual profile should be defined. The coordinate of the points on the calculated profile are represented as $Cj(x_{cj}, y_{cj})$, and the adjacent points on the actual defect profile are represented as $Aj(x_{aj}, y_{aj})$, where j=1,2,…,S1. S1 is a positive integer and stands for the total number of points on the calculated profile. The error e_j for each point group is defined as

$$e_j = \frac{|y_{cj} - y_{aj}| * \delta(|x_{cj} - x_{aj}|)}{y_{aj}} + \frac{|x_{cj} - x_{aj}| * \delta(|y_{cj} - y_{aj}|)}{x_{aj}}, \tag{9}$$

http://mc.manuscriptcentral.com/insi

where $\delta(x)$ is the unit impulse-like function and satisfies

$$\delta(x) = \begin{cases} 1, x = 0 \text{ or } x < \varepsilon \\ 0, x \neq 0 \text{ or } x \geq \varepsilon \end{cases}, \tag{10}$$

where ε is a user-selected parameter and it is a small positive number.

Based on the definition of the point error, the error between the calculated profile and the actual profile at each point is calculated. In order to clearly describe the error distribution, the error values are plotted on the dimension of the rectangular coordinate system, based on the coordinates of the actual defect profile, as shown in Fig. 6.

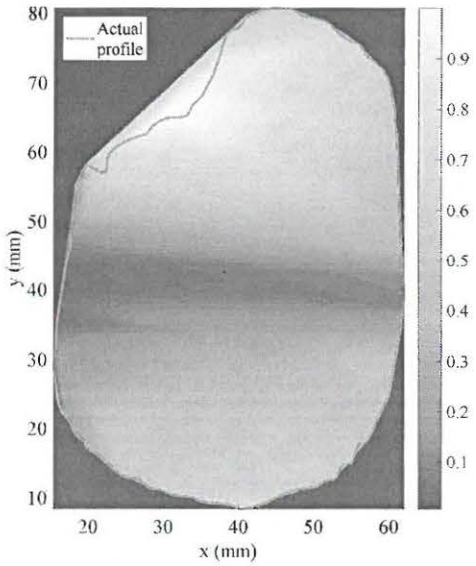

FIG. 6. The normalized error distribution between the calculated profile and the actual defect profile.

The normalized signal intensity near the actual defect profile in Fig. 6 represents the error between the calculated profile and the actual profile. Errors in the top-left area are obviously larger than those in other areas. The top-left area of the actual defect profile contains several inwardly recessed boundaries, which guided waves can hardly reach. So errors in these recessed boundaries are relatively large. Similar situations are fit for the bottom area of the actual defect profile, with several irregularly fluctuating boundaries. The normalized error

http://mc.manuscriptcentral.com/insi

distribution and analyzed reasons agree well with the result in Fig. 5, where the calculated profile deviates from the actual defect profile in a similar way.

In order to have an overall evaluation on the accuracy of the proposed profile imaging method, the average profile error E_a is defined based on the error for each point group:

$$E_a = \frac{1}{S1}\sum_{j=1}^{S1} e_j \tag{11}$$

The average profile error is calculated to be 4.3%, which indicates that the proposed profile imaging method can achieve fairly high-precision profile images for actual defects. However, the value of the average profile error is deteriorated by the relatively larger errors in the top-left area due to inwardly recessed boundaries, where the error reaches approximately 12% at some severely fluctuating points. The average profile error apart from these special areas is only 1.1%, which indicates high accuracy for the profile reconstruction for actual defects.

The proposed guided wave scattering model is proved to be able to accurately calculate the position of scattering point and the direction of scattering edge, which can essentially describe the local profile of the actual defect. The profile imaging method based on the scattering model exploits the EMAT array to collect enough information of the actual defect boundary to obtain the high-precision profile image.

6. Conclusions

This work proposes a profile imaging method aimed at actual defects in steel plate based on electromagnetic ultrasonic SH guided wave scattering. The scattering model is established on the rectangular coordinate system. The scattering point and the scattering edge are defined and calculated to materialize the scattering model. And the position of the scattering point is proved to be uniquely determined on the condition that the transmitting direction is known. Then the procedures of the profile imaging method exploiting the EMAT array are provided.

http://mc.manuscriptcentral.com/insi

The experimental platform on a steel plate with an actual defect is setup. Direction-controllable transmitters and omni-directional receivers based on SH guided waves are applied to stimulate and receive SH waves containing defect information. The proposed profile imaging method and procedures are performed on this experimental system and the profile image of the actual defect is obtained. Besides, the error between the calculated profile and the actual profile is defined and illustrated on the dimension of the rectangular coordinate system. Results show that the calculated profile is quite close to the actual one and the average profile error is only 4.3%. Therefore, the proposed guided wave scattering model and the profile imaging method are the major contribution of the work, and they are proved to be able to accurately describe the profile of the actual defect in steel plate.

Acknowledgments

This research was supported by the National Natural Science Foundation of China (NSFC) (No. 51277101, No. 51677093), the Royal Society-NSFC International Exchanges Award (No. IE150600), the Royal Academy of Engineering Newton Research Collaboration Program (No. NRCP/1415/91) and the Royal Academy of Engineering Distinguished Visiting Fellowship program (No. DVF1415/2/17).

References

1. R H Priewald, C Magele, P D Ledger, N R Pearson and J S D Mason, 'Fast magnetic flux leakage signal inversion for the reconstruction of arbitrary defect profiles in steel using finite elements', IEEE Transactions on Magnetics, Vol 49, No 1, pp 506-516, January 2013.
2. G B Kumbhar, S M Mahajan, and W L Collett, 'Reduction of loss and local overheating in the tank of a current transformer', IEEE Transactions on Power Delivery, Vol 25, No 4, pp 2519-2525, October 2010.

http://mc.manuscriptcentral.com/insi

3. A R Ramirez, J S D Mason, and N Pearson, 'Experimental study to differentiate between top and bottom defects for MFL tank floor inspections', NDT & E International, Vol 42, No 1, pp 16-21, January 2009.
4. J A de Raad, T Bouma, and A Bonisch, 'Rapid corrosion screening in up to 30 mm wall thickness for plates and pipe', Insight, Vol 44, No 2, pp 97-103, February 2002.
5. L Mazeika, R Kazys, R Raisutis and R Sliteris, 'Ultrasonic guided wave tomography for the inspection of the fuel tanks floor', International Journal of Materials & Product Technology, Vol 41, No 1-4, pp 128-139, 2011.
6. N Kasai, K Sekine, and H Maruyama, 'Influence of corrosion products on magnetic flux leakage signals in inspection of far-side metal-loss defects in oil storage tank bottom floors', Journal of the Japan Petroleum Institute, Vol 47, No 1, pp 19-26, January 2004.
7. S Zeroug, S Bose, B Sinha, M Skataric, Y Liu and R D'Angelo, 'Sonic and ultrasonic measurement applications for cased oil wells', Insight, Vol 58, No 8, pp 423-430, August 2016.
8. Q Wang, M Hong, and Z Q Su, 'An in-situ structural health diagnosis technique and its realization via a modularized system', IEEE Transactions on Instrumentation and Measurement, Vol 64, No 4, pp 873-887, April 2015.
9. P S Lowe, R Sanderson, N V Boulgouris, and T H Gan, 'Hybrid active focusing with adaptive dispersion for higher defect sensitivity in guided wave inspection of cylindrical structures', Nondestructive Testing and Evaluation, Vol 31, No 3, pp 219-234, September 2016.
10. D G Xiao, Q Fan, C G Xu, and X H Zhang, 'Measurement methods of ultrasonic transducer sensitivity', Ultrasonics, Vol 68, pp 150-154, May 2016.

http://mc.manuscriptcentral.com/insi

11. Z G Zhou, H X Zhao, G K Sun, P F He, J Fan, and G Li, 'Inspection of disbonds in multilayer dissimilar metal structure using lock-in thermography', Applied Optics, Vol 55, No 16, pp 4490-4496, June 2016.
12. C Huang, and X J Wu, 'An improved ferromagnetic material pulsed eddy current testing signal processing method based on numerical cumulative integration', NDT & E International, Vol 69, pp 35-39, January 2015.
13. T Hayashi, 'Imaging defects in a plate with complex geometries', Applied Physics Letters, Vol 108, No 8, pp 1-4, February 2016.
14. G Y Tian, Y L Gao, K J Li, Y Z Wang, B Gao, and Y Z He, 'Eddy current pulsed thermography with different excitation configurations for metallic material and defect characterization', Sensors, Vol 16, No 6, pp 1-11, June 2016.
15. L Y Yu, and Z H Tian, 'Guided wave phased array beamforming and imaging in composite plates', Ultrasonics, Vol 68, pp 43-53, May 2016.
16. W B Li, and Y Cho, 'Quantification and imaging of corrosion wall thinning using shear horizontal guided waves generated by magnetostrictive sensors', Sensors and Actuators A-Physical, Vol 232, pp 251-258, August 2015.
17. K Arunmuthu, M Ashish, T Saravanan, J Philip, B P C Rao, and T Jayakumar, 'Simulation of beam hardening in X-ray tomography and its correction using linearisation and pre-filtering approaches', Insight, Vol 55, No 10, pp 540-547, October 2013.
18. J C P McKeon, and M K Hinders, 'Parallel projection and crosshole lamb wave contact scanning tomography', Journal of the Acoustical Society of America, Vol 106, No 5, pp 2568-2577, November 1999.
19. J K Van Velsor, H Gao, and J L Rose, 'Guided-wave tomographic imaging of defects in pipe using a probabilistic reconstruction algorithm', Insight, Vol 49, No 9, pp 532-537, September 2007.

http://mc.manuscriptcentral.com/insi

20. W B Duan, R Kirby, and P Mudge, 'On the scattering of elastic waves from a non-axisymmetric defect in a coated pipe', Ultrasonics, Vol 65, pp 228-241, February 2016.
21. R M Levine, and J E Michaels, 'Block-sparse reconstruction and imaging for lamb wave structural health monitoring', IEEE Transactions on Ultrasonics Ferroelectrics and Frequency Control, Vol 61, No 6, pp 1006-1015, June 2014.
22. R M Levine, and J E Michaels, 'Model-based imaging of damage with Lamb waves via sparse reconstruction', Journal of the Acoustical Society of America, Vol 133, No 3, pp 1525-1534, March 2013.
23. J S Hall, P Fromme, and J E Michaels, 'Guided Wave Damage Characterization via Minimum Variance Imaging with a Distributed Array of Ultrasonic Sensors', Journal of Nondestructive Evaluation, Vol 33, No 3, pp 299-308, September 2014.
24. J L Rose, S Pelts, and Y Cho, 'Modeling for flaw sizing potential with guided waves', Journal of Nondestructive Evaluation, Vol 19, No 2, pp 55-66, June 2000.
25. A Demma, P Cawley, M Lowe, A G Roosenbrand, and B Pavlakovic, 'The reflection of guided waves from notches in pipes: a guide for interpreting corrosion measurements', NDT & E International, Vol 37, No 3, pp 167-180, April 2004.
26. Y Cho, 'Estimation of ultrasonic guided wave mode conversion in a plate with thickness variation', IEEE Transactions on Ultrasonics Ferroelectrics and Frequency Control, Vol 47, No 3, pp 591-603, 2000.
27. T E Michaels, J E Michaels, and M Ruzzene, 'Frequency-wavenumber domain analysis of guided wavefields', Ultrasonics, Vol 51, No 4, pp 452-466, May 2011.
28. Y Zhang, S L Huang, S Wang, and W Zhao, 'Time-frequency energy density precipitation method for time-of-flight extraction of narrowband lamb wave detection signals', Review of Scientific Instruments, Vol 87, No 5, pp 1-8, June 2016.

http://mc.manuscriptcentral.com/insi

29. Y Zhang, S L Huang, S Wang, and W Zhao, 'Direction-controllable electromagnetic acoustic transducer for SH waves in steel plate based on magnetostriction', Progress In Electromagnetics Research M, Vol 50, No 1, pp 151-160, September 2016.

http://mc.manuscriptcentral.com/insi